JMEPEG (2016) 25:3948–3959
DOI: 10.1007/s11665-016-2247-5

1059-9495/$19.00

Preparation and Performance of Plasma/Polymer Composite Coatings on Magnesium Alloy

H.R. Bakhsheshi-Rad, E. Hamzah, S. Bagheriyan, M. Daroonparvar, M. Kasiri-Asgarani, A.M. Shah, and M. Medraj

(Submitted December 28, 2015; in revised form May 30, 2016; published online July 29, 2016)

A triplex plasma (NiCoCrAlHfYSi/Al_2O_3·13%TiO_2)/polycaprolactone composite coating was successfully deposited on a Mg-1.2Ca alloy by a combination of atmospheric plasma spraying and dip-coating techniques. The NiCoCrAlHfYSi (MCrAlHYS) coating, as the first layer, contained a large number of voids, globular porosities, and micro-cracks with a thickness of 40-50 µm, while the Al_2O_3·13%TiO_2 coating, as the second layer, presented a unique bimodal microstructure with a thickness of 70-80 µm. The top layer was a hydrophobic polymer, which effectively sealed the porosities of plasma layers. The results of microhardness and bonding strength tests showed that the plasma coating presented excellent hardness (870 HV) and good bonding strength (14.8 MPa). However, the plasma/polymer coatings interface exhibited low bonding strength (8.6 MPa). The polymer coating formed thick layer (100-110 µm) that homogeneously covered the surface of the plasma layers. Contact angle measurement showed that polymer coating over plasma layers significantly decreased surface wettability. The corrosion current density (i_{corr}) of an uncoated sample (262.7 µA/cm^2) decreased to 76.9 µA/cm^2 after plasma coatings were applied. However, it was found that the i_{corr} decreased significantly to 0.002 µA/cm^2 after polymer sealing of the porous plasma layers.

Keywords corrosion behavior, hydrophobic properties, mechanical properties, Mg alloy, triplex coating

1. Introduction

Applications of Mg-based alloys have significantly increased in the aviation and automobile industries because of a combination of unique low density and physical and mechanical properties (Ref 1-3). However, the application of Mg alloys has been hindered because of their low corrosion resistance that causes them to lose functionality during service in a corrosion-active media (Ref 4-6). Apart from alloying, surface treatments such as plasma electrolytic oxidation (PEO), ion implantation, micro-arc oxidation (MAO), anodic oxidation, atmospheric plasma spraying (APS), and polymer coatings are feasible methods of retarding the corrosion of Mg alloys (Ref 5-8). Atmospheric plasma spraying (APS), a fast and an environmentally friendly process, is an effective coating method for ceramic coating (Ref 9). Alumina-based coatings can significantly improve wear resistance and provide good corrosion protection and thermal insulation (Ref 10). The addition of TiO_2 can improve both the toughness and wear resistance of an Al_2O_3 coating (Ref 9, 11). It has been demonstrated that an Al_2O_3·13%TiO_2 (AT) coating presented better properties, such as wear properties, compared to other AT coatings (Ref 9). In this regard, the use of a bond coat such as MCrAlY (M=Ni,Co) or NiCrAlY decreases the thermal expansion coefficient mismatch between the ceramic top coat and the substrate, increases the adhesion of the top coating to the Mg substrate, and prevents debonding (Ref 12, 13). Moreover, MCrAlY coatings have superior hot corrosion resistance and more ductility and fatigue resistance than aluminide coatings (Ref 14). In this regard, it was reported that even addition of small amounts of Hf and Y leads to significant increase in adhesion of alumina scales. In addition, a plasma-sprayed AT coating contained a large number of microdefects, porosity, and micro-cracks, which allow an aggressive solution to penetrate the coating during service resulting in corrosion of magnesium alloy (Ref 9, 15). Tian et al. (Ref 16) demonstrated that, in plasma-sprayed AT coatings, corrosion mainly occurred at the substrate near the MCrAlY (M = Ni,Co) bond coating/substrate interface. Wang et al. (Ref 17) showed that a plasma-sprayed AT coating suffered from permeable defects in the coating, leading to an accelerating corrosion rate. Thus, top coatings should be employed to seal the pores of plasma coatings and to improve corrosion performance. Polymer coating is an effective approach for sealing the porosity of plasma layers to avoid the early failure of plasma coatings. Among the polymer coatings, polycaprolactone (PCL; –[$(CH_2)_5COO]_n$–), a

H.R. Bakhsheshi-Rad and **M. Kasiri-Asgarani,** Advanced Materials Research Center, Department of Materials Engineering, Islamic Azad University, NajafAbad Branch, NajafAbad, Iran; **E. Hamzah**, Department of Materials, Manufacturing and Industrial Engineering, Faculty of Mechanical Engineering, Universiti Teknologi Malaysia, 81310 Johor Bahru, Johor, Malaysia; **S. Bagheriyan**, Department of Geology, Shahriyar Branch, Islamic Azad University, Shahriyar, Iran; **M. Daroonparvar**, Department of Materials, Manufacturing and Industrial Engineering, Faculty of Mechanical Engineering, Universiti Teknologi Malaysia, 81310 Johor Bahru, Johor, Malaysia; and Department of Materials Engineering, Faculty of Engineering, Islamic Azad university, Roudehen Branch, Roudehen, Tehran, Iran; and Center for Engineering Operations Management, Department of Technology and Innovation, University of Southern Denmark, Odense M-5230, Denmark; **A.M. Shah**, Medical Devices and Technology Group, Faculty of Bioscience and Medical Engineering, Universiti Teknologi Malaysia, 81310 Skudai, Johor Bahru, Johor, Malaysia; and **M. Medraj**, Department of Mechanical Engineering, Concordia University, 1455 De Maisonneuve Blvd. West, Montreal, QC H3G 1M8, Canada; and Mechanical and Materials Engineering, Masdar Institute, PO Box 54224, Abu Dhabi, UAE. Contact e-mails: rezabakhsheshi@ gmail.com and bhamidreza2@live.utm.my.

semicrystalline linear hydrophobic polymer, is considered a promising candidate because of its good mechanical properties, such as the high ductility of 80% elongation at the break point (Ref 18, 19). In addition, a PCL coating acts as the top layer on a porous plasma layer to fill its porosity and further improves the corrosion resistance of the substrate (Ref 18-20). Polymer coatings are commonly employed to enhance the protective performance of plasma spray, micro-arc oxidation (MAO), and plasma electrolytic oxidation (PEO) coatings (Ref 1, 19-21). In view of this, Ivanou et al. (Ref 1) exhibited that sealing of a PEO coating with an epoxy-silane layer significantly enhanced the corrosion protection of a magnesium ZE41 alloy. It has also been found that sealing a porous PEO coating with superdispersed polytetrafluoroethylene (SPTFE) considerably enhanced the protective properties of the surface of a magnesium alloy MA8 (Ref 2). However, the sealing of plasma-sprayed MCrAlHYS/-nano-AT coatings with a hydrophobic PCL polymer coating has not been reported yet. Thus, in the present study, combinations of APS and dip coatings were conducted to provide a triple-layer MCrAlHYS/nano-AT/PCL coating system that integrates the advantages of both methods. The effectiveness of the triple-layer composite coating on the mechanical properties and corrosion behavior of an Mg-Ca alloy has also been investigated.

2. Experimental Details

Magnesium alloys with dimensions of 15 mm × 10 mm × 10 mm were used as a substrate. A commercial NiCoCrAlHfYSi (MCrAlHYS; Ni22Co17Cr12Al0.5Hf0.5Y0.4Si; Amdry 386) powder ranging in size from 60-70 μm and an agglomerated nanostructured Al_2O_3-13%TiO_2 powder (Nanox S2613S; Inframat Corporation, USA) were used as the first layer and second layer, respectively. It should be mentioned that single nanoparticles cannot be sprayed because of their low mass and inertia. To address this issue, the reconstitution of the nanoparticles into micrometer-sized granules is vital (Ref 12). As shown in Fig. 1a, the MCrAlHYS feedstock powder particles have a spherical morphology that is suitable for plasma spray. However, AT powder has a porous microstructure with particles ranging in size from 80 to 500 nm (Fig. 1b). The mapping of the elements on the surface of AT powder consisted predominantly of Al, O, and Ti (Fig. 1c). For better adhesion of the coating, the surface of magnesium alloy was blasted with alumina particles, and the specimens were subsequently rinsed with acetone. An atmospheric plasma spray (METCO, type 3MB) was used for plasma spraying of the MCrAlHYS and nanostructured AT powders. For plasma spray, argon (Ar) was employed as primary plasma operating gas and hydrogen (H_2) was employed as an auxiliary gas. In this regard, Ar flow rate was 60 L/min; H_2 flow rate, 8 L/min; voltage, 50 V; and current, 500 A. The spray distance was kept at 12 and 10 cm for MCrAlHYS and AT coatings, respectively. Nitrogen was used as powder feed gas, and the powder feed rate was about 15 and 20 g/min for MCrAlHYS and AT coatings, respectively.

Prior to the dipping of MCrAlHYS and MCrAlHYS/AT, 2.5 wt.% PCL pellets (M_w = 80,000 g/mol, Sigma-Aldrich, UK) were dissolved in dichloromethane (DCM; CH_2Cl_2, Sigma-Aldrich, UK) by stirring for 6 h at room temperature. The samples were dipped for 30 s and withdrawn at a constant speed to form a uniform coating and then dried at room temperature.

Compressive tests were carried out before and after immersion in 3.5 wt.% NaCl for 10 days and then cleaned in a boiling solution of chromium trioxide (CrO_3) to remove the surface corrosion products. The specimens were then dried in warm air. For compressive tests, the standard samples were prepared according to ASTM E9, using an Instron-5569 universal testing machine at a displacement rate of 0.5 mm/min at ambient temperature. For each testing condition, two specimens were examined. The bonding strength of the coated

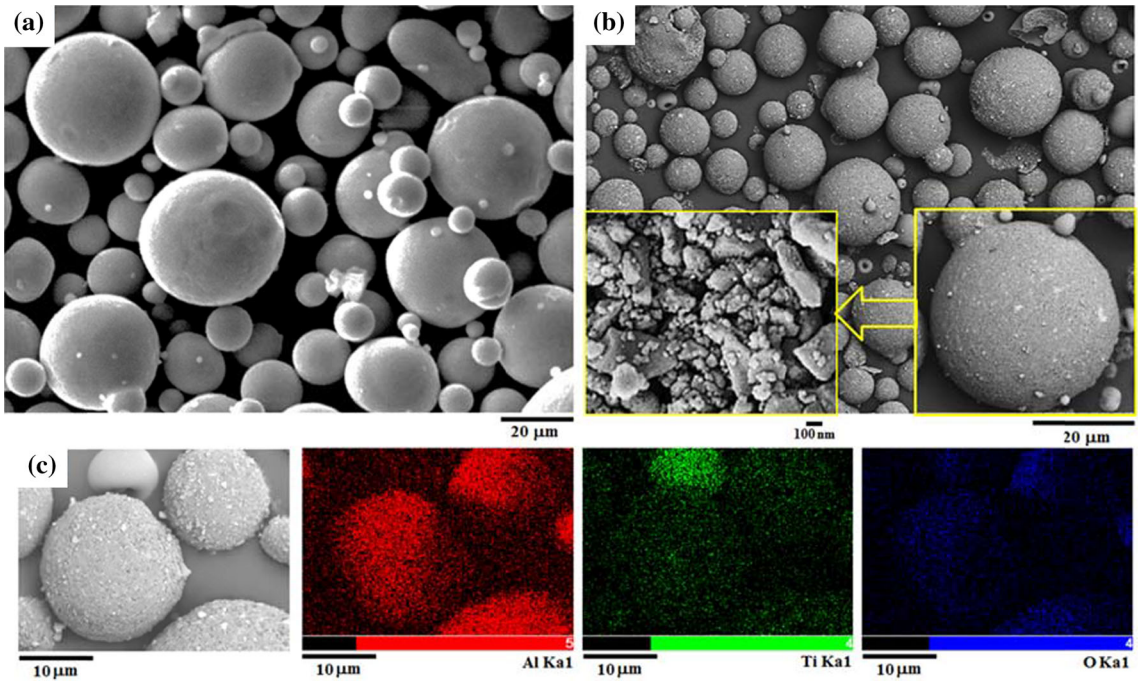

Fig. 1 Surface morphology of (a) MCrAlHYS powders, (b) agglomerated nano-AT powders, and (c) elemental mapping of agglomerated nano-AT powders

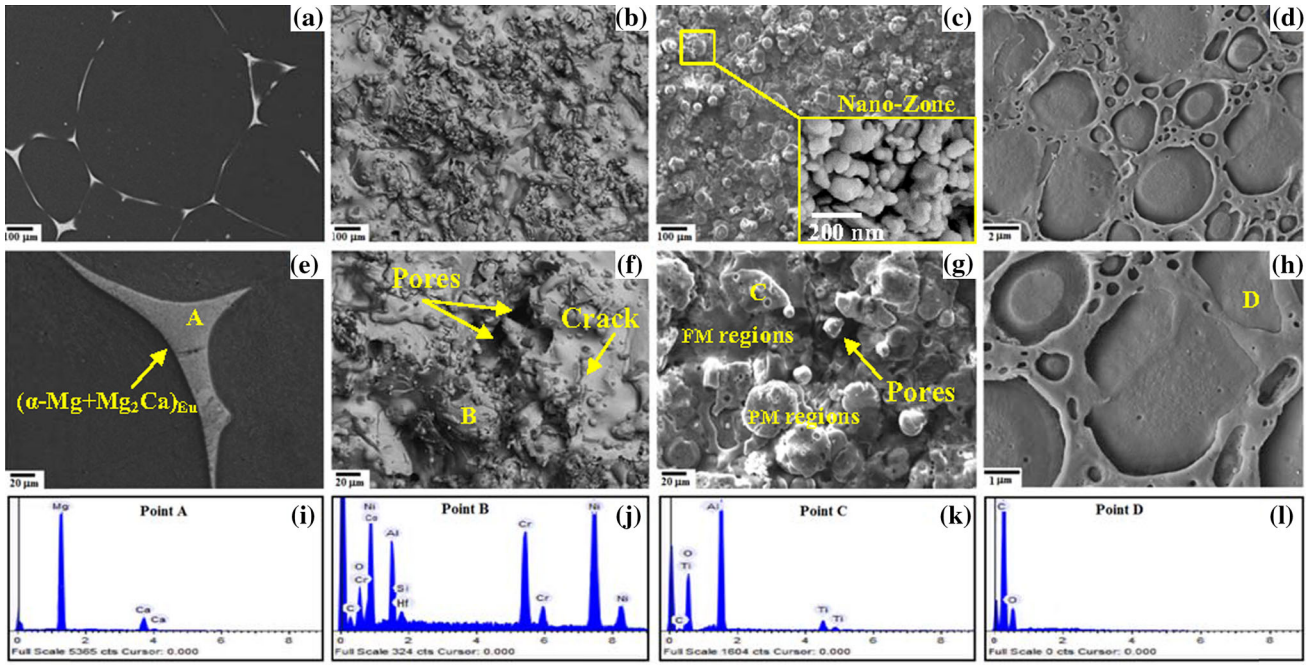

Fig. 2 Surface morphology of (a, e) uncoated Mg alloy, (b, f) single-layer MCrAlHYS coating, (c, g) bilayer MCrAlHYS/nano-AT coating, and (d, h) triple-layer MCrAlHYS/nano-AT/PCL-coated Mg alloy and EDS analysis of (i) point A, (j) point B, (k) point C, and (l) point D (PM: partially melted; FM: fully melted)

specimens was measured according to the ASTM F1044 standard using a universal testing machine (Instron 5569). Cylindrical specimens with the dimensions of 30 mm × 10 mm were prepared. The crosshead displacement rate was 1 mm/min with a 10 kN load cell. Three composite-coated specimens were tested, and the average value was reported. The average microhardness (n = 5) of the plasma-sprayed coated alloys was measured from the cross section using a Vickers hardness tester (Shimadzu) using a 500 g for 15 s. For electrochemical testing, rectangular specimens with a surface area of 1 cm^2 were mounted in epoxy resin, and the tests were conducted in an open-air glass cell containing 350 mL 3.5 wt.% NaCl, using a PARSTAT 2263 potentiostat/galvanostat (Princeton Applied Research). A three-electrode cell was used for potentiodynamic polarization testing. The reference electrode was a saturated calomel electrode (SCE), the counter electrode was a graphite rod, and the specimen was the working electrode. The samples were immersed in the NaCl solution for 1 h prior to the PDP test to establish the open-circuit potential. All experiments were carried out at a constant scan rate of 0.5 mV/s, initiated at –250 mV relative to the open-circuit potential. The electrochemical impedance spectra (EIS) were measured over a frequency range of 1 Hz to 100 kHz using a VersaSTAT 3 machine. Each electrochemical test was repeated to confirm the reproducibility of the results. Immersion testing was carried out according to ASTM G1-03. Specimens with a diameter of 10 mm and thickness of 10 mm were immersed in a beaker containing 200 mL of 3.5 wt.% NaCl solution for 10 days. The immersion tests were repeated at least once to verify the reproducibility of the results. An x-ray diffractometer (Siemens-D5000) was used to evaluate the phase transformation using Cu-Kα radiation (λ = 1.5405 Å) generated at 35 kV and 25 mA over the 2θ range of 20°–90° with increment steps of 0.04. Microstructures were analyzed with scanning electron microscopy (JEOL JSM-6380LA) equipped with an EDS system (JEOL Inc., Tokyo, Japan) and transmission electron microscopy (HT7700 Hitachi). Hydrophobic properties of uncoated and coated samples were evaluated by measuring static contact angles of a water droplet placed on the sample surfaces using automatically video-based optical contact angle (VCA Optima, AST Products Inc.,) at ambient temperature with a water droplet of about 1 μL. The average value of five measurements at different positions was determined as the contact angle for each sample.

3. Results and Discussion

3.1 Characterization of the Coating

Figure 2 shows SEM images of uncoated alloy, a single-layer plasma coating (MCrAlHYS/AT), a bilayer plasma coating (MCrAlHYS/AT), and a triple-layer plasma/polymer coating (MCrAlHYS/AT/PCL). The uncoated Mg–1.2Ca alloy consists of an Mg_2Ca intermetallic compound in addition to α-Mg matrix that is consistent with the Mg–Ca phase diagram (Ref 22) (Fig. 2a, e). The presence of a secondary phase can significantly affect the corrosion behavior of the Mg alloy because of the formation of micro-galvanic cells between the matrix and secondary phases (Ref 23-25). The corresponding EDS analysis in the denoted area further confirms that the grain boundaries contain measurable amount of calcium, which indicates the formation of Mg_2Ca (Fig. 2i). The single-layer and bilayer plasma coatings contained pores, voids, and micro-cracks because of the residual stresses that occur during the deposition process (Fig. 2b, c, f, g) (Ref 26). The presence of an intermediate MCrAlHYS layer provides good mechanical bonding between Mg substrate and AT layer, which has a significant effect on the corrosion behavior of the Mg alloy. However, the bilayer coating presented a more compact layer

with fewer pores and micro-cracks than the single-layered coating (Fig. 2c, g). The presence of these pinholes, interconnected porosities, and micro-cracks in the plasma coatings provides pathways for the infiltration of aggressive solution into the coating during corrosion (Ref 27). An EDS analysis showed a high amount of Ni, Al, and Cr accompanied with a low Y, Hf, and Si content, indicating the formation of a MCrAlHYS coating (Fig. 2j). However, the nanostructure AT coating is composed of Al, O, and Ti (Fig. 2k). The polymer coating (PCL) over the MCrAlHYS/AT layers indicated a sealed pore structure with a relatively uniform distribution. The top polymer layer consists of sealed micropores and voids in the plasma coating (Fig. 2d, h). The EDS analysis (Fig. 2l) also resulted in the detection of C and O in this sample, indicating the formation of a PCL film. The cross-sectional morphology (Fig. 3a) shows a MCrAlHYS coating with a thickness of approximately 40-50 μm formed on the surface of the magnesium alloy. A large number of voids, globular porosities, and micro-cracks can also be observed. However, two-layer structure can be seen (Fig. 3b) that contains AT layer with a thickness of 70-80 μm as the second layer and MCrAlHYS as the first layer. It can be observed that there are some micropores in the plasma layers (MCrAlHYS/AT) because these layers are generally porous, resulting in more penetration of aggressive solutions into the coating during corrosion. In addition, the AT coating consists of both fully melted and partially melted regions, a result in agreement with the bimodal microstructure found in the literature (Ref 28). Fully melted regions have a columnar structure. In contrast, partially melted regions (PM) consist of solid-phase sintered regions and some equiaxed grains (Ref 10). It has been reported (Ref 29) that submicron grains are Al_2O_3-rich particles and that the thin net walls belong to a TiO_2-rich matrix microstructure. This observation is mainly related to the selective melting of TiO_2 nanoparticles during air plasma spraying. In contrast, remaining nanoparticles that belong to the solid-phase sintered regions can be easily observed (Ref 10). The remaining nanoparticles have nearly not grown in comparison with the internal microstructure of the original powder. The PCL coating indicates the formation of thick layers (100-110 μm) that homogeneously cover the surface of the MCrAlHYS/AT layers (Fig. 3c). It can also be observed that the PCL layer has good bonding with the AT plasma layer.

Figure 4 shows TEM micrographs and a selected area electron diffraction (SAED) pattern of the nano-AT coating. Figure 4a depicts part of the fully melted (FM) region, mainly composed of γ-Al_2O_3. Luo et al. (Ref 30) demonstrated that the FM region is composed approximately of the metastable γ-Al_2O_3 phase, confirmed by the presence of splat morphology, which can only be obtained through melting and rapid solidification. The SAED shows a ring pattern related to the fully melted splat structure which mainly consisted of γ-Al_2O_3 (Fig. 4c). In contrast, Fig. 4b shows part of the partially melted region, which represents the three-dimensional net structure of the α-Al_2O_3. The size of submicron grain α-Al_2O_3 ranges from 100 to 800 nm, and it is embedded in a γ-Al_2O_3 matrix. Furthermore, some inter-granular cracks can be found in coatings formed during the plasma spray process owing to the residual stresses (Ref 31). The SAED further confirmed that the grains mainly consisted of α-Al_2O_3 grains (Fig. 4d). The SAED of the inter-granular layers close to the grain showed that the inter-granular layers had an amorphous structure (32).

The XRD patterns (Fig. 5a) of the uncoated sample show the formation of the Mg_2Ca compounds. The plasma coating (MCrAlHYS) contains γ phase (Ni, Cr-rich), γ′ phase (Ni_3AL), and $AlCr_3$ phase peaks and some traces of β phase (AlNi) peaks (Fig. 5b). However, the bilayer plasma coating (AT) is composed of γ-Al_2O_3, brookite-TiO_2, and α-Al_2O_3. The presence of prominent α-Al_2O_3 peaks in the coating may originate from the partially melted regions in the bimodal structure of the coating (Ref 30, 33). The top surface of the triple-layer coating (MCrAlHYS/AT/PCL) consists of two

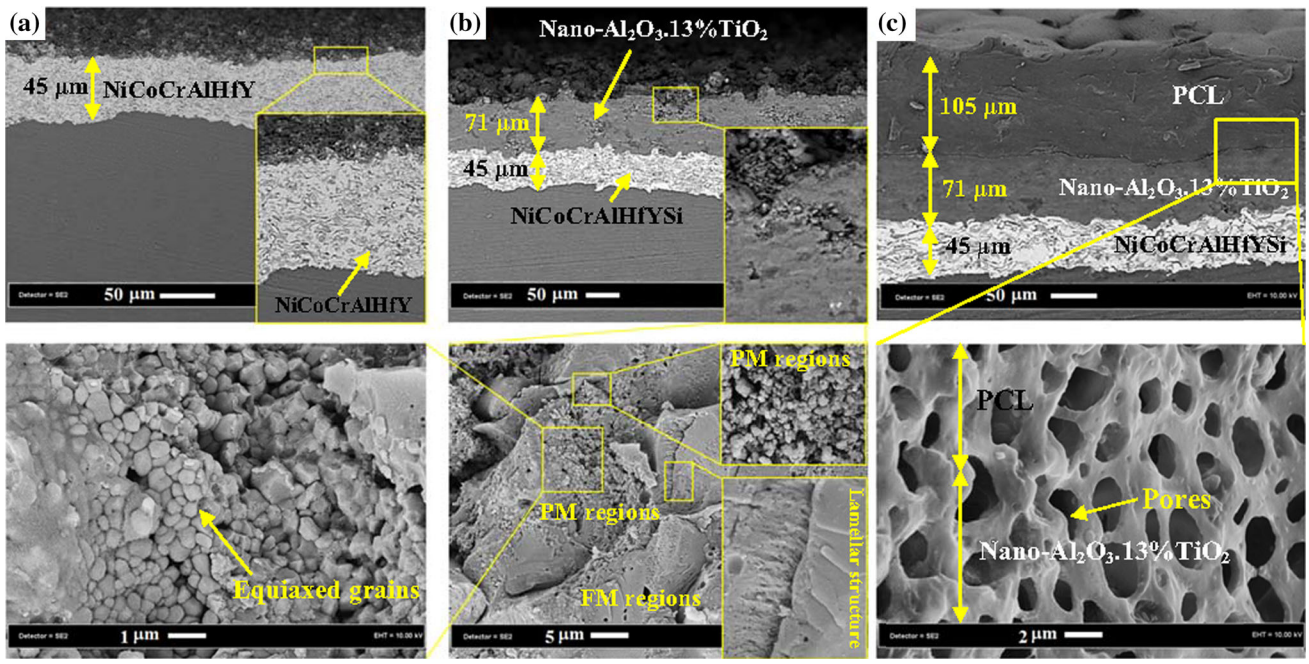

Fig. 3 Cross-sectional SEM micrographs of (a) single-layer MCrAlHYS, and (b) bilayer MCrAlHYS/nano-AT and (c) triple-layer MCrAlHYS/-nano-AT/PCL-coated Mg alloy (PM: partially melted; FM: fully melted)

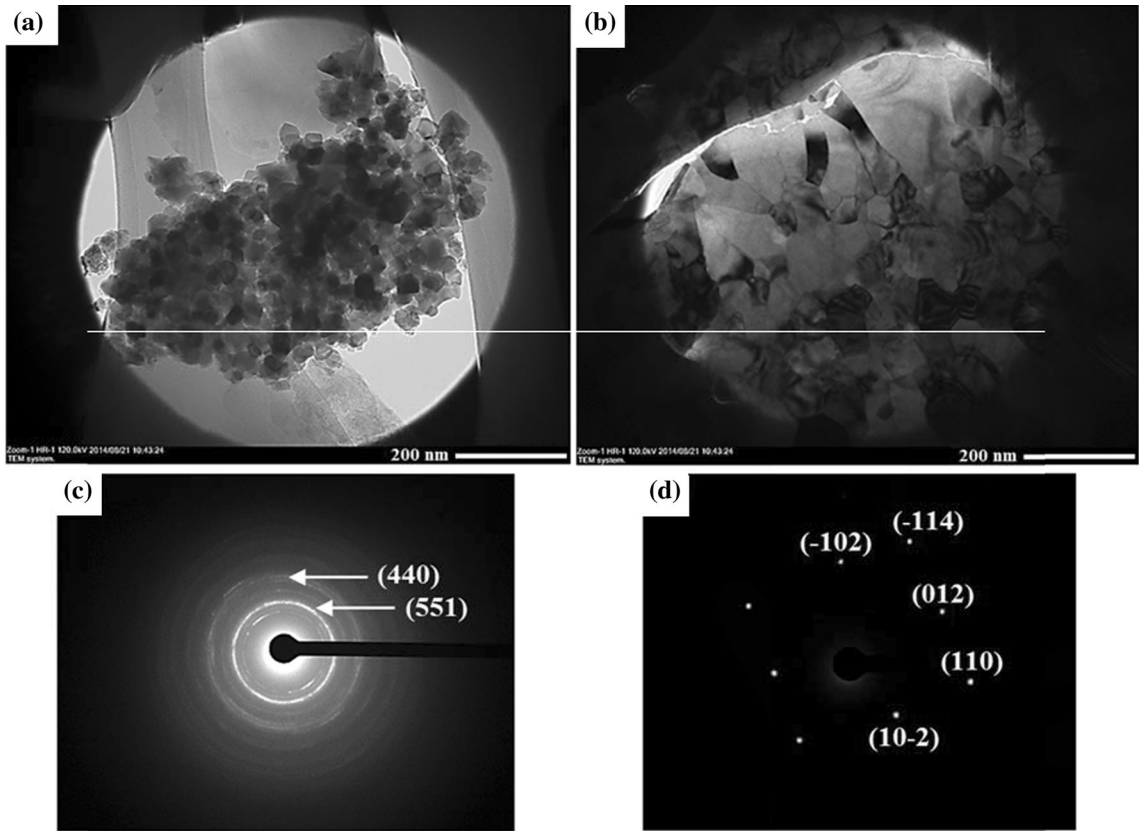

Fig. 4 TEM micrographs with selected area diffraction pattern of (a) nanocrystalline γ-Al_2O_3 in the FM region, (b) large grains of α-Al_2O_3 embedded in the PM region, (c) SADP of γ-Al_2O_3 crystals, and (d) SADP of α-Al_2O_3

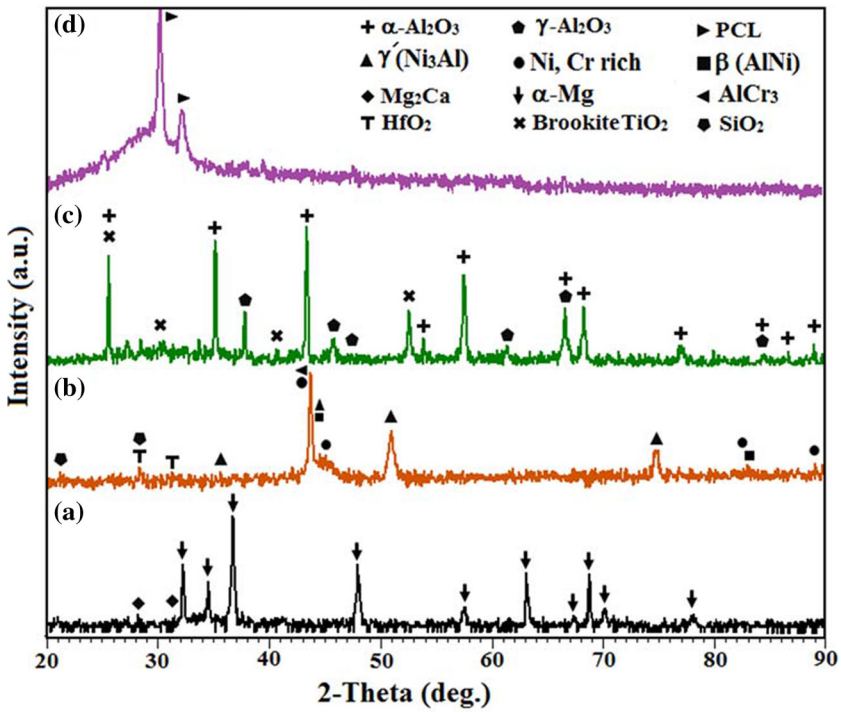

Fig. 5 X-ray diffraction patterns of (a) uncoated, (b) MCrAlHYS coating, (c) nano-AT coating, and (d) PCL-coated Mg alloy

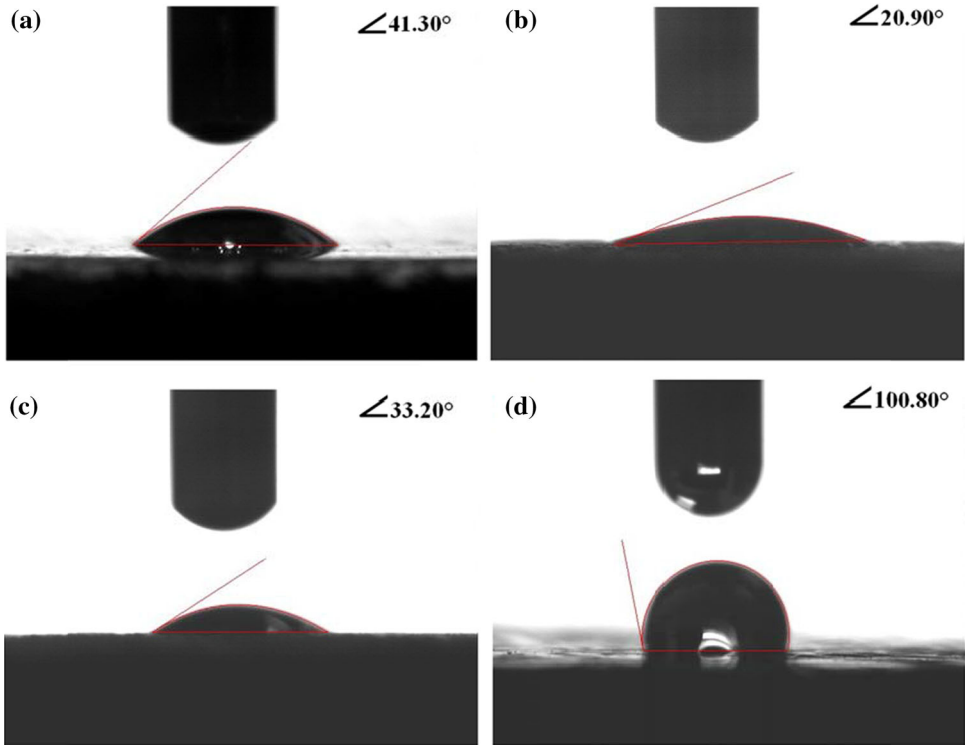

Fig. 6 Images of water contact angle on (a) single-layer MCrAlHYS, (b) bilayer MCrAlHYS /nano-AT, and (c) triple-layer MCrAlHYS/nano-AT/PCL-coated Mg alloy

Table 1 Compression test results of the uncoated Mg-1.2Ca alloy, single-layer MCrAlHYS-coated, dual-layer MCrAlHYS/AT-coated, and triple-layer MCrAlHYS/AT/PCL-coated Mg alloy before and after immersion in 3.5 wt.% NaCl solution

Specimen	Uncoated Mg alloy before immersion	Uncoated Mg alloy after 10-day immersion	MCrAlHYS-coated alloy after 10-day immersion	MCrAlHYS/AT-coated alloy after 10-day immersion	MCrAlHYS/AT/PCL-coated alloy after 10-day immersion
Compression strength—UCS, MPa	234.7 ± 15	159.3 ± 6	179.8 ± 8	189.1 ± 9	215.2 ± 12

UCS ultimate compressive strength

intense peaks at $2\theta = 21.6°$ and $2\theta = 23.8°$, accounting for diffraction on the 110 and 200 planes, respectively. PCL has a crystalline structure with polyethylene-like orthorhombic cell disposition, with lattice parameters $a = 0.748$ nm, $b = 0.498$ nm, and $c = 1.727$ nm (Ref 34).

The contact angle of the uncoated, plasma-coated, and plasma-/polymer-coated samples is shown in Fig. 6. As can be seen, the uncoated Mg-Ca sample has a hydrophilic surface with contact angle of 41.30° (Fig. 6a). It can be also observed that the surfaces of the single-layer plasma coating (MCrAlHYS) and the bilayer plasma coating (MCrAlHYS/AT) are hydrophilic, as the water droplet easily wets and spreads out over the plasma-coated surface. However, polymer-coated sample indicated hydrophobic behavior as the water droplet forms a large contact angle (Ref 35). The static contact angles on the single and bilayer plasma-coated sample are 20.90° and 33.20°, respectively, which allows the water droplet to spread over the surface and quickly penetrate into the substrate (Fig. 6b, c) (Ref 36). In contrast, triple-layer plasma-/polymer-coated sample presented hydrophobic properties with a contact angle of 100.80° (Fig. 6d), indicating that the hydrophobic nature strongly depends on the nature of the top coating. This phenomenon indicates that the polymer coating over plasma layer can effectively diminish the contact area with an aqueous solution, which is expected to significantly improve the corrosion resistance.

3.2 Mechanical Properties

The compressive strength of uncoated and coated samples before and after immersion in 3.5 wt.% NaCl solution for 10 days (Table 1) showed that Mg samples coated with a combination of plasma and polymer presented the highest compressive strengths (215.2 MPa) after 10 days of immersion in NaCl solution. This can be taken to indicate that the polymer coating can seal the porosity of plasma layers, so the transportation of corrosive ions (Cl^-) and electrolyte was

largely blocked. Therefore, it can be stated that a strong protective barrier was obtained by the plasma/polymer coating (Ref 32). However, both plasma-coated samples indicated lower compressive strength. This is because the porous structure of the plasma coating could not protect the substrate against corrosion because of the presence of pores in the structure of the plasma layers, allowing corrosive species water to easily diffuse through these defects and set up a galvanic cell at the interface of the substrate and the MCrAlHYS layer (Fig. 7). In this galvanic cell, the Mg alloy is an anode and the MCrAlHYS is cathodic, so the Mg alloy corroded significantly. With further infiltration of the solution into the plasma layer, more corrosion occurred, which leads to more corrosion products formed at the plasma/substrate interface, which destroyed the adhesion of the plasma layer to the substrate and debonded the coating, subsequently compromising the protective effect of the coating. The uncoated sample presented the lowest compressive strength (159.3 MPa) after immersion in NaCl solution, which is attributed to the occurrence of galvanic reactions between the α-Mg and the Mg_2Ca phases as the specimen was immersed in the solution. Figure 8 shows that the MCrAlHYS/AT coating (870 HV) is approximately 19 times harder than the uncoated alloy (45.4 HV). The higher hardness values of AT coating compared to the MCrAlHYS coating are due to the presence of semi-molten nanostructured particles that are embedded in the AT structure, which act as crack arresters, thereby increasing coating toughness (Ref 33, 37). In MCrAlHYS coating, a crack propagates *via* the coating's weakest link, which is the well-defined layered structure such as the splat boundaries. The bonding strength of the plasma coating (MCrAlHYS/AT) is higher (14.8 MPa) than that of the polymer/plasma coating (MCrAlHYS/AT/PCL). This is caused by the mechanical interlocking of the splats to the asperities of the substrate.

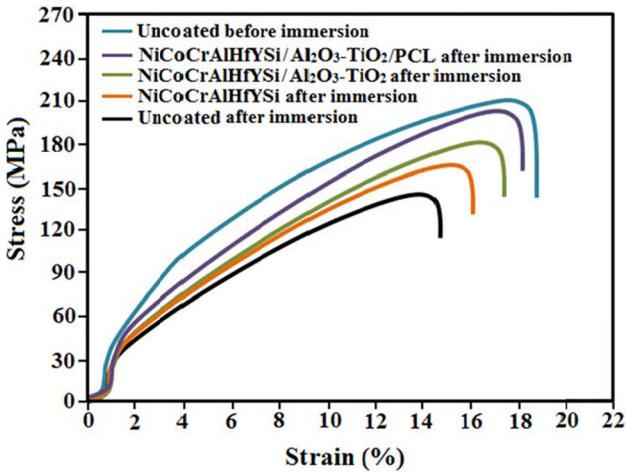

Fig. 7 Compressive stress–strain curves of uncoated, MCrAlHYS, MCrAlHYS/nano-AT, and MCrAlHYS/nano-AT/PCL-coated Mg alloy before and after immersion in 3.5 wt.% NaCl solution for 10 days

3.3 Electrochemical Corrosion Behavior

The electrochemical polarization curves of the uncoated, plasma-, and plasma-/polymer-coated samples in NaCl solution are shown in Fig. 9. The corrosion potential (E_{corr}) of the uncoated samples (–1613.5 mV_{SCE}) shifted to the nobler direction after monolayer coating (–901.4 mV_{SCE}), bilayer plasma coating (–814.7 mV_{SCE}), and plasma/polymer coatings (–1257.6 mV_{SCE}). In accordance with the mixed standard electrode potential theory (Ref 38), it was found that the air plasma spray-coated samples were nobler than the uncoated Mg alloy. The uncoated alloy presented the highest corrosion current density (i_{corr}) compared to the coated alloy owing to the formation of a micro-galvanic cell between the Mg_2Ca phase and the α-Mg phase. However, the plasma/polymer coating sample presented a lower i_{corr} (0.002 μA/cm^2) than the single-layer (2.68 μA/cm^2) and bilayer plasma-coated samples (1.75 μA/cm^2). Because of the formation of galvanic corrosion between the Mg substrate and the plasma layer through porosities and micro-cracks, which absorb the corrosive solution, the plasma layer cannot sufficiently protect the Mg substrate. This result is in accordance with (Ref 39). However, after polymer coating over the plasma layer, the porosities of the plasma coating can be sealed and interrupt the penetration of the corrosive species, resulting in a significant decrease in the corrosion rate of the plasma-/polymer-coated sample. A

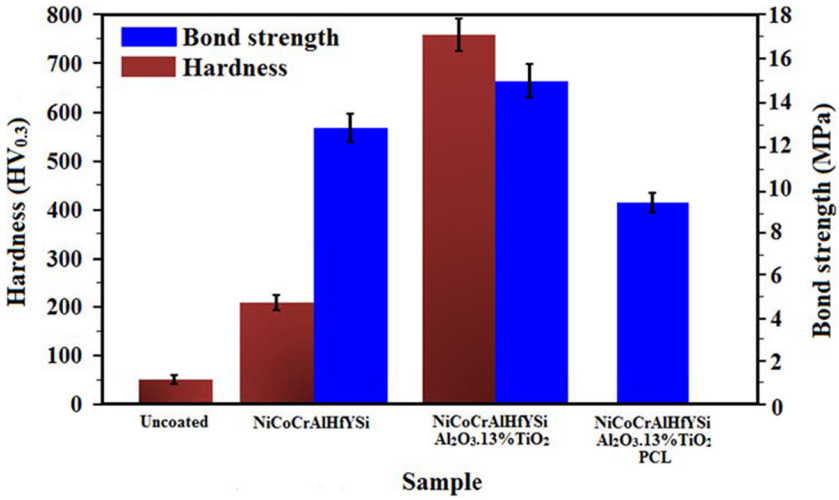

Fig. 8 Bond strength and hardness of uncoated, MCrAlHYS, MCrAlHYS/nano-AT coated, and MCrAlHYS/nano-AT/PCL coated on Mg alloy

corresponding increase in polarization resistance (R_P) from 1.26 kΩ·cm^2 (for the uncoated alloy) to 5.09, 6.88, and 729.3 kΩ·cm^2 for the single-layer, bilayer plasma, and triple-layer plasma/polymer coatings, respectively, was encountered (Table 2). Similarly, plasma/polymer coatings presented lower corrosion rates (P_i) than the plasma-coated and uncoated samples. This is thought to indicate that the PCL can seal the pores and voids in the plasma layer, which can prevent penetration of the electrolyte through the AT coating.

Nyquist plots of coated and uncoated specimens showed a typical single-capacitive semicircle (Fig. 10a), which represents the electrochemical process with only one time constant (Ref 20). The EIS spectra of uncoated sample can be fitted well using a simple equivalent circuit (Model A) as shown in Fig. 10b which is composed of the double-layer capacitance, Q_{dl}, in parallel with the charge transfer resistance, R_{ct}, to represent the interface between the electrolyte and Mg alloy. EIS spectra from coated Mg samples should in principle be fitted by $R[QR]$, but the best fit is obtained by using a four-component model (Model B) which gave a better fit. In this circuit, R_e represents the solution resistance, Q_c is the coating capacitance, R_p is the coating pore resistance, and R_{ct} is the charge transfer resistance which is attributed to the electrochemical corrosion activity at the interface. In general, the high charge transfer resistance indicates that the sample has good corrosion resistance. The charge transfer resistance (R_t) of the uncoated magnesium alloy (1.53 kΩ·cm^2) increased to 2094.32 kΩ·cm^2 in polymer/plasma, 2.64 kΩ·cm^2 in bilayer, and 2.28 kΩ·cm^2 in single-layer coated samples. This indicates that a high level of corrosion protection of the Mg substrate can be provided by polymer/plasma coating by sealing the porosities and blocking the ionic transport in the plasma coating, including chloride ion penetration through pores and subsequently the formation of a galvanic cell (40).

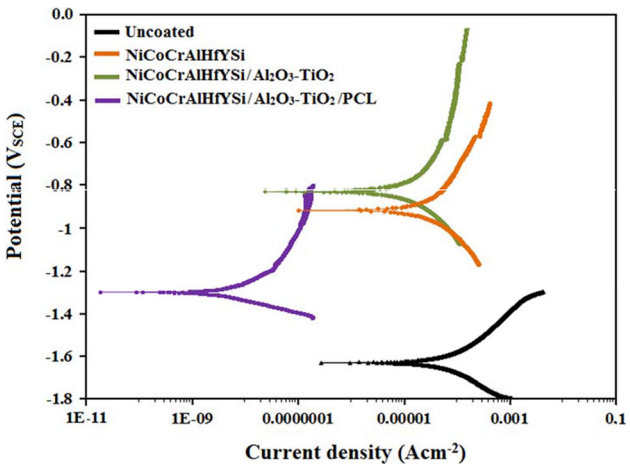

Fig. 9 Potentiodynamic polarization curves of uncoated, plasma-coated, and plasma-/polymer-coated Mg alloy specimens in 3.5 wt.% NaCl solution

The Bode plots of the EIS spectra show that polymer/plasma coating presented the best corrosion protective behavior, as their impedance modulus at low frequency ($|Z|$) value is the highest (Fig. 10c). The polymer coating sealed the porosity of the plasma coating and improved barrier performance for protection of the substrate against corrosion. However, the plasma coatings and the uncoated samples presented lower $|Z|$ compared to the triple-layer coatings at the low-frequency limit, which was attributed to the corrosion susceptibility of these samples. The combination of polarization and impedance tests shows that the triple-layer (MCrAlHYS/AT/PCL) coating efficiently delays the penetration of electrolyte through the coating and thus enhances the barrier performance of the coating. The Bode phase plot of uncoated and plasma-coated and plasma-/polymer-coated samples indicated that (Fig. 10d) the aperture of the phase angle increased after applying the plasma/polymer coatings on the magnesium alloy substrate. This is due to the protective performance of the plasma/polymer coatings. However, the uncoated alloy presented small phase angle and the aperture of the phase angle decreased, because the surface film cannot protect the substrate effectively. These results showed that plasma/polymer triple coating acts as an effective barrier layer to protect the Mg alloy substrate against NaCl solution.

3.4 Surface Characterization After Corrosion

Figure 11 shows the surface morphology of uncoated, plasma-coated, and plasma-/polymer-coated samples after soaking in 3.5 wt.% NaCl solution for 240 h. The micrograph of the bare Mg alloy samples exhibited that the surface microstructure did undergo serious corrosion damage since several pitting corrosion regions and cracks were found in the alloy. It is also clear that the corrosion product is formed on the sample surface of the uncoated sample (Fig. 11a, e). This corrosion product, according to the EDS analysis, mainly consists of Mg and O which implied the formation of $Mg(OH)_2$. However, both plasma coatings demonstrate fewer cracks and smaller pits. In this regard, MCrAlHYS coating undergoes severe localized corrosion on its surface accompanied with accumulation of large amount of corrosion products (Fig. 11b, f). Meanwhile, the MCrAlHYS/AT coating suffers from much milder localized corrosion and lower amount of

Table 2 Analysis results of Tafel polarization curves of uncoated Mg-Ca alloy, single-layer MCrAlHYS, dual-layer MCrAlHYS/AT, and triple-layer MCrAlHYS/AT/PCL-coated Mg alloy in 3.5 wt.% NaCl solution obtained from the polarization test

Alloy	Corrosion potential, E_{cor}, mV vs. SCE	Current density, i_{corr}, μA/cm^2	Cathodic slope, $-\beta_C$, mV/decade vs. SCE	Anodic slope, β_a, mV/decade vs. SCE	Polarization resistance, R_P, kΩcm^2	Corrosion rate, P_i, mm/year
Mg alloy	–1613.5 ± 15	262.7 ± 8	102 ± 5	90 ± 5	1.26 ± 0.13	6.00 ± 0.4
MCrAlHYS coated	–901.4 ± 9	117.6 ± 5	298 ± 9	245 ± 8	5.09 ± 0.35	2.68 ± 0.3
MCrAlHYS/AT coated	–814.7 ± 8	76.9 ± 3	302 ± 9	242 ± 8	6.88 ± 0.46	1.75 ± 0.2
MCrAlHYS/AT/PCL coated	–1257.6 ± 10	0.12 ± 0.03	392 ± 11	133 ± 6	729.3 ± 16	0.002 ± 0.001

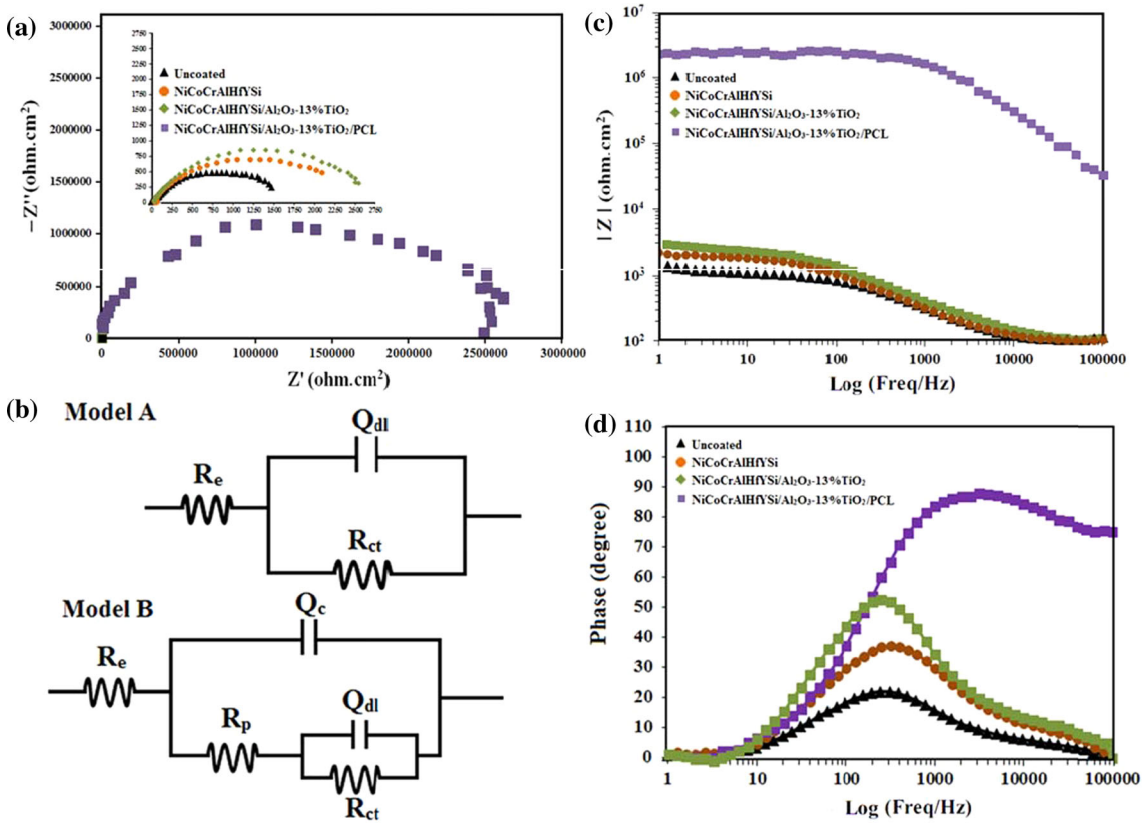

Fig. 10 Electrochemical impedance spectroscopy measurements of uncoated and coated Mg alloy. (a) Nyquist plot, (b) equivalent electrical circuit for uncoated (Model A) and coated samples (Model B), (c) Bode plot, and (d) Bode phase plot

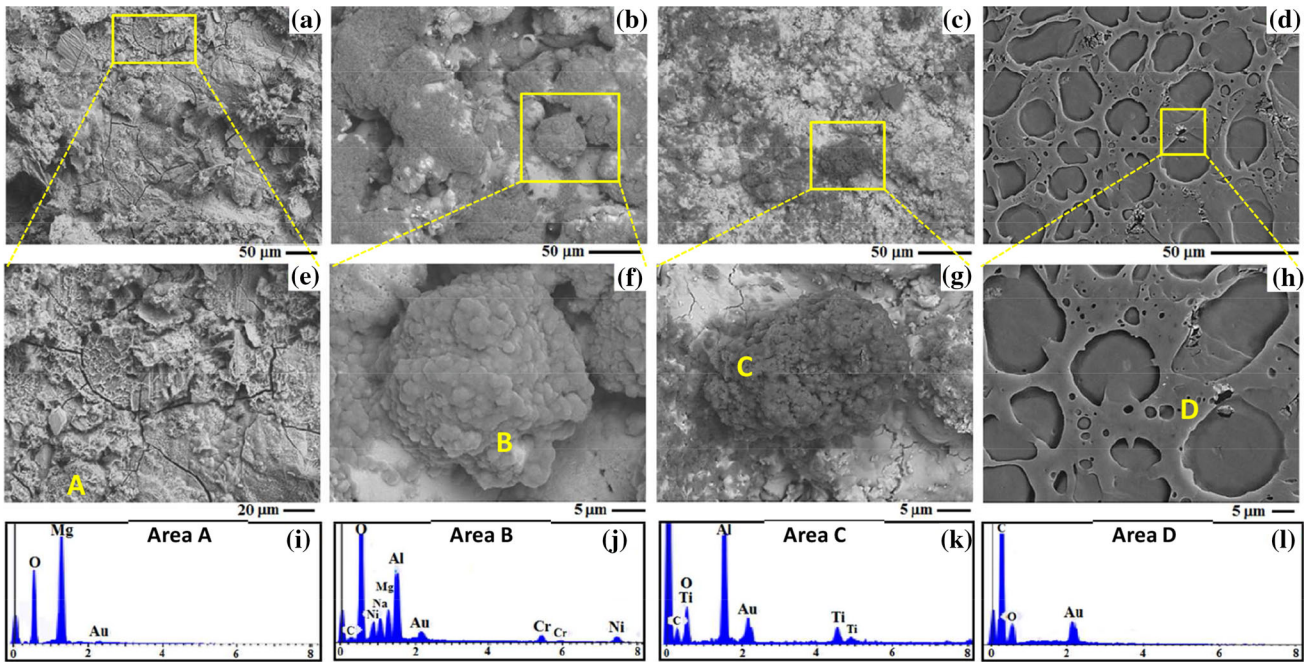

Fig. 11 FESEM micrographs of (a, e) uncoated Mg–Ca alloy, (b, f) MCrAlHYS coating, (c, g) MCrAlHYS/nano-AT coating, and (d, h) MCrAlHYS/nano-AT/PCL-coated Mg alloy after immersion in 3.5 wt.% NaCl solution for 240 h and EDS analysis of (i) area A, (j) area B, (k) area C, and (l) area D

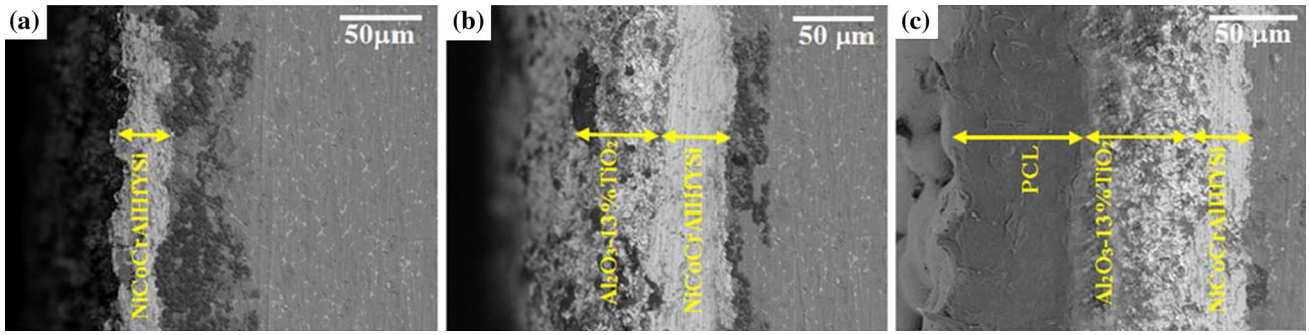

Fig. 12 Cross-sectional SEM micrographs of (a) single-layer MCrAlHYS, (b) bilayer MCrAlHYS/nano-AT, and (c) triple-layer MCrAlHYS/nano-AT/PCL-coated Mg alloy after immersion in 3.5 wt.% NaCl solution for 10 days

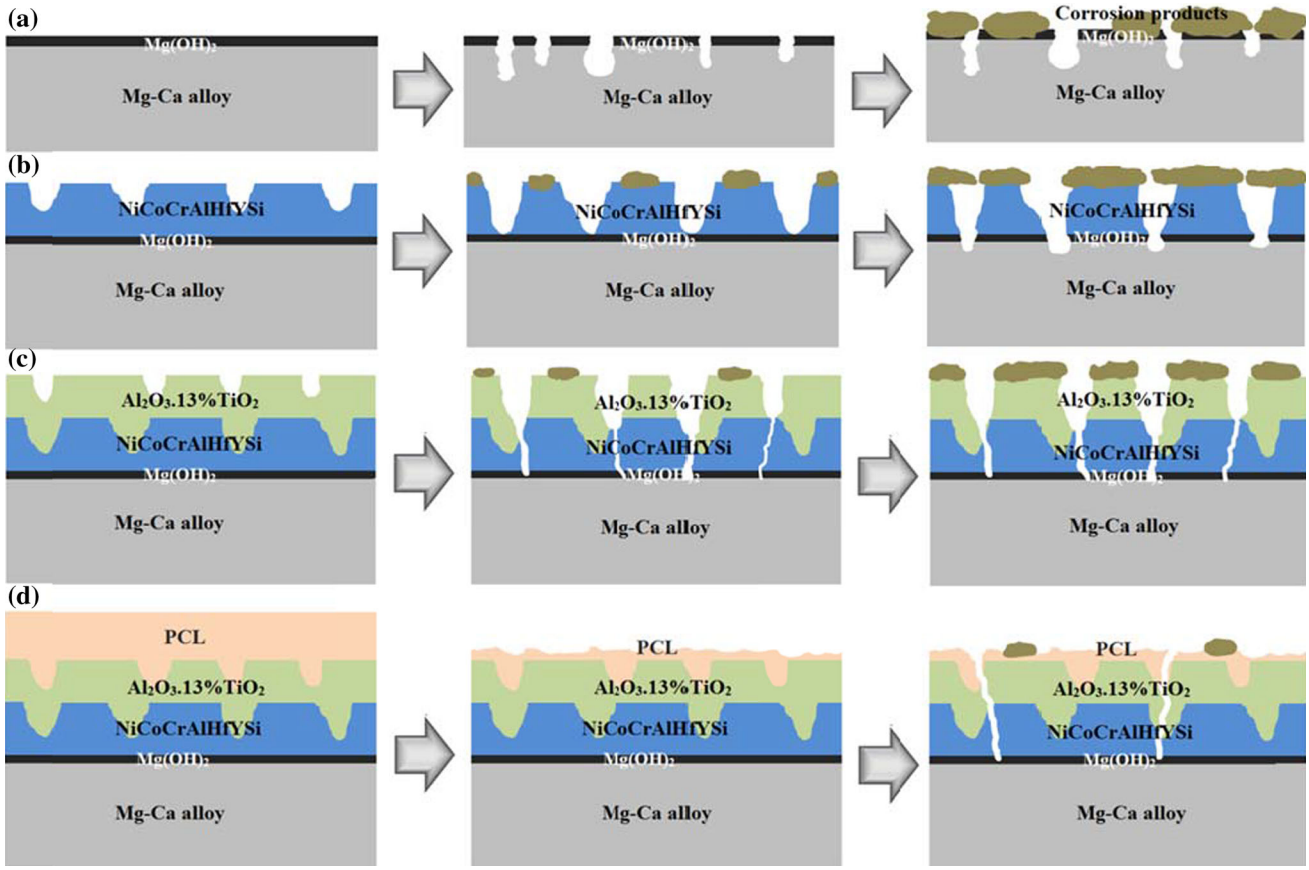

Fig. 13 Schematic illustration of the corrosion mechanism of (a) uncoated Mg-Ca alloy, (b) single-layer MCrAlHYS, (c) dual-layer MCrAlHYS/nano-AT, and (d) triple-layer MCrAlHYS/nano-AT/PCL-coated Mg alloy after immersion in 3.5 wt.% NaCl solution for 240 h

corrosion products, indicating that double-layer coating presents better corrosion protection from uncoated Mg alloy (Fig. 11c, g). EDS analysis of plasma-coated samples indicates that the corrosion products with globular morphology in Fig. 11(j, k) consist of certain amount of $Mg(OH)_2$ and $Al(OH)_3$. However, the SEM macrostructure of the triple-layer coating (Fig. 11d, h) indicates that there is no sign of serious corrosion damage in the polymer layer except for a few dark corrosion sites and small cracks which further confirm its corrosion protection ability. The presence of these sites can be attributed to the generation of hydrogen according to the following reaction: $2H_2O + 2e^- \rightarrow H_2\uparrow + 2OH^-$. Hydrogen gas could have been trapped at the polymer/plasma interface which led to escalating hydrogen pressure underneath the polymer layer and thus blistering of polymer layer (Ref 41). With passage of time, the hydrogen pressure increased, resulting in damaging of the polymer layer and leaving dark corrosion sites on the polymer layer. In EDS analysis, a peak of C and O corresponded to the PCL, indicating that the polymer structure remained unchanged and further confirmed that polymer coating over plasma layers can effectively protect the Mg substrate.

The SEM micrographs of the cross sections of single-layer, double-layer and triple-layer coated samples after immersion in

3.5 wt.% NaCl solution for 10 day are exhibited in Fig. 12. The triple-layer coated sample experiences slight corrosion attack since the presence of PCL film as overlayer on the plasma layer provides more protection for the substrate as it reduces the corrosion attack and the plasma layers (underlayer) protect the substrate from the aggressive solution when it passes through from the overlayer. On the other hand, the double layer revealed lower damage as small areas of the plasma/substrate interface were corroded only. This can be attributed to the formation of more compact coating and presence of lesser amount of pores, voids, and micro-cracks in double-layer coated sample compared to the single-layer coated sample. However, single-layer coated sample seriously suffers from the corrosion attack compared with the double- and triple-layer samples, and extended areas with localized corrosion at the coating/substrate interface were observed.

The corrosion mechanisms of the uncoated and coated Mg–1.2Ca alloy are schematically exhibited in Fig. 13. As bare Mg alloy was exposed to 3.5 wt.% NaCl solution (Fig. 13a), the grain boundaries were preferentially corroded due to the micro-galvanic activity between Mg_2Ca secondary phase and magnesium. At the same time as a result of the occurrence of electrochemical reactions on the Mg alloy surface, a thin layer of $Mg(OH)_2$ was formed. In this regard, the corrosion rate slightly decreased due to the formation of protective $Mg(OH)_2$ layer and gradually forming corrosion products. However, this protective layer can be destroyed due to the presence of the aggressive Cl^- ions and eventually transforming it into more soluble $MgCl_2$. With passage of time, the amount of localized corrosion becomes increasingly pronounced, resulted in formation of several big pits indicating rapid corrosion of bare Mg alloy. However, the single-layer MCrAlHYS coating presented some protection against corrosion attack during the initial exposure period (Fig. 13b). The porous nature of plasma layer provides passage for the infiltration of chloride ions to the interface of plasma layer/substrate, which led to debonding of the plasma layer to the substrate and losing the protection effect of the coating. Formation of these corrosion products at the interface of the plasma layer/substrate introduced stress to the surroundings which damaged the plasma layer. Double-layer MCrAlHYS/AT coating can provide more protection than single-layer coating due to the presence of lower amount of micropores and micro-flaws (Fig. 13c). Micropores act as channels for the Cl^- corrosive ions and further penetration of the solution to the inner porous plasma layer (MCrAlHYS) and formation of a strong galvanic cell between the Mg alloy and the plasma layer (Ref 42–45) as a result of a large difference in corrosion potential (Ref 10, 12). However, the triple-layer coating MCrAlHYS/AT/PCL provided strong protective barrier film against penetration of solution containing relatively high chloride concentration (Fig. 13d). PCL as top layer fully covered the surface of plasma layer and significantly inhibited the penetration of the electrolyte. In this regard, it should be mentioned that the pitting corrosion was not observed even after 240 h of exposure to NaCl solution. The polarization curve and EIS result further confirmed less infiltration of the solution because the R_p was considerably higher for the triple-layer coating compared to single-layer and double-layer coatings. However with increasing exposure time, the PCL layer starts to dissolve, and as a consequence of the degradation of PCL, the solution containing chloride reaches the porous plasma layer and the substrate which leads to decrease in the protection effect of the coating.

4. Conclusion

A triplex MCrAlHYS/AT/PCL coating system was fabricated on a Mg-1.2Ca alloy by a combination of atmospheric plasma spraying (APS) and dip-coating methods. The first layer was MCrAlHYS with a thickness of 40-50 μm, and the second layer was nano-AT, while the top layer was hydrophobic PCL with a thickness of 100-110 μm. MCrAlHYS/AT/PCL coatings demonstrated high compressive strength after immersion in 3.5 wt.% NaCl for 10 days. A maximum contact angle of 100.80° was measured on the PCL. It was demonstrated that the PCL coating effectively sealed the porous MCrAlHYS/AT coatings and prevented the penetration of corrosive solutions through the AT coating. The study showed that a PCL coating can significantly enhance the corrosion resistance of the plasma-coated Mg alloy.

Acknowledgments

The author(s) would like to thank the Malaysian Ministry of Higher Education (MOHE) and Universiti Teknologi Malaysia for providing the financial support and facilities for this research.

References

1. D.K. Ivanou, M. Starykevich, A.D. Lisenkov et al., Plasma anodized ZE41 magnesium alloy sealed with hybrid epoxy-silane coating, *Corros. Sci.*, 2013, **73**, p 300–308
2. S.V. Gnedenkov, S.L. Sinebryukhov, D.V. Mashtalyar et al., Composite polymer-containing protective coatings on magnesium alloy MA8, *Corros. Sci.*, 2014, **85**, p 52–59
3. J. Zhou, Q. Li, H. Zhang, and F. Chen, Corrosion behavior of AZ91D magnesium alloy in three different physiological environments, *J. Mater. Eng. Perform.*, 2014, **23**, p 181–186
4. N.G. Wang, R.C. Wang, C.Q. Peng, and Y. Feng, Corrosion behavior of magnesium alloy AP65 in 3.5 % sodium chloride solution, *J. Mater. Eng. Perform.*, 2012, **21**, p 1300–1308
5. E. Ghali, W. Dietzel, and K.U. Kainer, General and localized corrosion of magnesium alloys: a critical review, *J. Mater. Eng. Perform.*, 2013, **22**, p 2875–2891
6. M.C. Lopes de Oliveira, V.S. Marques Pereira, O.V. Correa, and R.A. Antunes, Corrosion performance of anodized AZ91D magnesium alloy: effect of the anodizing potential on the film structure and corrosion behavior, *J. Mater. Eng. Perform.*, 2014, **23**, p 593–603
7. M. Daroonparvar, M.A.M. Yajid, N.M. Yusof et al., Investigation of three steps of hot corrosion process in Y_2O_3 stabilized ZrO_2 coatings including nano zones, *J. Rare Earths*, 2014, **32**, p 989–1002
8. H.R. Bakhsheshi-Rad, E. Hamzah, S. Farahany, and M. Staiger, The Mechanical Properties and Corrosion Behavior of Quaternary Mg–6Zn–0.8Mn–xCa Alloys, *J. Mater. Eng. Perform.*, 2015, **24**, p 598–608
9. D. Wang, Z. Tian, S. Wang, L. Shen, and Z. Liu, Microstructural characterization of Al_2O_3–13 wt.% TiO_2 ceramic coatings prepared by squash presetting laser cladding on GH4169 superalloy, *Surf. Coat. Technol.*, 2014, **254**, p 195–201
10. H. Jamali, R. Mozafarinia, R. Shoja-Razavi, and R. Ahmadi-Pidani, Comparison of hot corrosion behaviors of plasma-sprayed nanostructured and conventional YSZ thermal barrier coatings exposure to molten vanadium pentoxide and sodium sulfate, *J. Eur. Ceram. Soc.*, 2014, **34**, p 485–492
11. Y. Chen, D. Wu, G. Ma, W. Lu, and D. Guo, Coaxial laser cladding of Al_2O_3-13%TiO_2 powders on Ti–6Al–4 V alloy, *Surf. Coat. Technol*, 2013, **228**, p S452–S455
12. X. Fan, Y. Liu, Z. Xu, Y. Wang et al., Preparation and Characterization of 8YSZ Thermal Barrier Coatings on Rare Earth-Magnesium Alloy, *J. Therm. Spray Technol.*, 2011, **20**, p 948–957

13. X. Fan, B. Zou, L. Gu, C. Wang, Y. Wang et al., Investigation of the bond coats for thermal barrier coatings on Mg alloy, *Appl. Surf. Sci.*, 2013, **265**, p 264–273
14. K.A. Unocic and B.A. Pint, Characterization of the alumina scale formed on a commercial MCrAlYHfSi coating, *Surf. Coat. Technol.*, 2010, **205**, p 1178–1182
15. C. Wang, B. Jiang, M. Liu, and Y. Ge, Corrosion characterization of micro-arc oxidization composite electrophoretic coating on AZ31B magnesium alloy, *J. Alloys Compd.*, 2015, **621**, p 53–61
16. W. Tian, Y. Wang, T. Zhang, and Y. Yang, Sliding wear and electrochemical corrosion behavior of plasma sprayed nanocomposite Al_2O_3–13%TiO_2 coatings, *Mater. Chem. Phys.*, 2009, **118**, p 37–45
17. Y. Wang, W. Tian, T. Zhang, and Y. Yang, Microstructure, spallation and corrosion of plasma sprayed Al_2O_3–13%TiO_2 coatings, *Corros. Sci.*, 2009, **51**, p 2924–2931
18. E.J. Lee, S.H. Teng, T.S. Jang, P. Wang et al., Nanostructured poly(ε-caprolactone)–silica xerogel fibrous membrane for guided bone regeneration, *Acta Biomater.*, 2010, **6**, p 3557–3565
19. H.M. Wong, K.W.K. Yeung, K.O. Lam et al., A biodegradable polymer-based coating to control the performance of magnesium alloy orthopaedic implants, *Biomaterials*, 2010, **31**, p 2084–2096
20. C. Zhou, X. Lu, Z. Xin, J. Liu, and Y. Zhang, Polybenzoxazine/SiO_2 nanocomposite coatings for corrosion protection of mild steel, *Corros. Sci.*, 2014, **80**, p 269–275
21. F.Y. Teng, I.C. Tai, M.W. Wang et al., The structures, electrochemical and cell performance of titania films formed on titanium by micro-arc oxidation, *J. Taiwan Inst. Chem. Eng*, 2014, **45**, p 1331–1337
22. M. Mezbahul-Islam, Y.N. Zhang, C. Shekhar, and M. Medraj, Critical assessment and thermodynamic modeling of Mg–Ca–Zn system supported by key experiments, *Calphad*, 2014, **46**, p 134–147
23. H.Y. Tok, E. Hamzah, and H.R. Bakhsheshi-Rad, The role of bismuth on the microstructure and corrosion behavior of ternary Mg–1.2Ca–*x*Bi alloys for biomedical applications, *J. Alloys Compd.*, 2015, **640**, p 335–346
24. M. Daroonparvar, M.A.M. Yajid, N.M. Yusof et al., Microstructural characterization and corrosion resistance evaluation of nanostructured Al and Al/AlCr coated Mg–Zn–Ce–La alloy, *J. Alloys Compd.*, 2014, **615**, p 657–671
25. H.R. Bakhsheshi-Rad, M.H. Idris, M.R.A. Kadir, and S. Farahany, Microstructure analysis and corrosion behavior of biodegradable Mg–Ca implant alloys, *Mater. Des.*, 2012, **33**, p 88–97
26. R. Ghasemi, R.S. Razavi, R. Mozafarinia, and H. Jamali, The influence of laser treatment on thermal shock resistance of plasma-sprayed nanostructured yttria stabilized zirconia thermal barrier coatings, *Ceram. Int.*, 2014, **40**, p 347–355
27. H.R. Bakhsheshi-Rad, E. Hamzah, M.R. Abdul-Kadir, S.N. Saud, M. Kasiri-Asgarani, and R. Ebrahimi-Kahrizsangi, The mechanical properties and corrosion behavior of double-layered nano hydroxyapatite–polymer coating on Mg–Ca alloy, *J. Mater. Eng. Perform.*, 2015, **24**, p 4010–4021
28. M.R.L. Estarki, H. Edris, R.S. Razavi et al., Spray drying of nanometric SYSZ powders to obtain plasma sprayable nanostructured granules, *Ceram. Int.*, 2013, **39**, p 9447–9457
29. D. Wang, Z. Tian, L. Shen, Z. Liu, and Y. Huang, Microstructural characteristics and formation mechanism of Al_2O_3–13 wt.% TiO_2 coatings plasma-sprayed with nanostructured agglomerated powders, *Surf. Coat. Technol.*, 2009, **203**, p 1298–1303
30. H. Luo, D. Goberman, L. Shaw, and M. Gell, Indentation fracture behavior of plasma-sprayed nanostructured Al_2O_3–13wt.%TiO_2 coatings, *Mater. Sci. Eng. A*, 2003, **346**, p 237–245
31. W. Tian, Y. Wang, Y. Yang, and C. Li, Toughening and strengthening mechanism of plasma sprayed nanostructured Al_2O_3–13 wt.%TiO_2 coatings, *Surf. Coat. Technol.*, 2009, **204**, p 642–649
32. C.G. Li, Z.S. Yu, Y.F. Zhang, P.L. Zhang, H. Yan et al., Microstructure evolution of laser remelted Al_2O_3–13 wt.%TiO_2 coatings, *J. Alloys Compd.*, 2013, **576**, p 187–194
33. R.S. Lima and B.R. Marple, Thermal spray coatings engineered from nanostructured ceramic agglomerated powders for structural, thermal barrier and biomedical applications: a review, *J. Therm. Spray Technol*, 2007, **16**, p 40–63
34. M. Lebourg, J.S. Antón, and J.L.G. Ribelles, Characterization of calcium phosphate layers grown on polycaprolactone for tissue engineering purposes, *Compos. Sci. Technol.*, 2010, **70**, p 1796–1804
35. X.J. Cui, X.Z. Lin, C.H. Liu et al., Fabrication and corrosion resistance of a hydrophobic micro-arc oxidation coating on AZ31 Mg alloy, *Corros. Sci.*, 2015, **90**, p 402–412
36. H.R. Bakhsheshi-Rad, E. Hamzah, A.F. Ismail et al., Synthesis and corrosion behavior of a hybrid bioceramic–biopolymer coating on biodegradable Mg alloy for orthopaedic implants, *J. Alloys Compd.*, 2015, **648**, p 1067–1071
37. C. Lamuta, G. Di Girolamo, and L. Pagnotta, Microstructural, mechanical and tribological properties of nanostructured YSZ coatings produced with different APS process parameters, *Ceram. Int.*, 2015, **41**, p 8904–8914
38. G. Wu, A. Shanaghi, Y. Zhao, X. Zhang et al., The effect of interlayer on corrosion resistance of ceramic coating/Mg alloy substrate in simulated physiological environment, *Surf. Coat. Technol.*, 2012, **206**, p 4892–4898
39. H.R. Bakhsheshi-Rad, E. Hamzah, M.R.A. Kadir et al., Corrosion and mechanical performance of double-layered nano-Al/PCL coating on Mg–Ca–Bi alloy, *Vacuum*, 2015, **119**, p 95–98
40. M. Sababi, J. Pan, P.E. Augustsson, P.E. Sundell, and P.M. Claesson, Influence of polyaniline and ceria nanoparticle additives on corrosion protection of a UV-cure coating on carbon steel, *Corros. Sci.*, 2014, **84**, p 189–197
41. H.R. Bakhsheshi-Rad, E. Hamzah, A.F. Ismail et al., Microstructural, mechanical properties and corrosion behavior of plasma sprayed NiCrAlY/nano-YSZ duplex coating on Mg–1.2Ca–3Zn alloy, *Ceram. Int.*, 2015, **41**, p 15272–15277
42. B.S. Boroujeny, Design and investigation of TiO2-SiO2 thin films on AISI 316L stainless steel for tribological properties and corrosion protection, *J. Adv. Mater. Process*, 2015, **3**, p 13–24
43. M. Daroonparvar, M.A. Mat Yajid, N.M. Yusof, H.R. Bakhsheshi-Rad, E. Hamzah, Improvement of corrosion resistance of binary Mg-Ca alloys by using duplex aluminum-chromium coatings, *J. Mater. Eng. Perform*, 2015, **24**, p 2614–2627
44. H.R. Bakhsheshi-Rad, E. Hamzah, M.R.A. Kadir et al., The mechanical properties and corrosion behavior of double-layered nano hydroxyapatite–polymer coating on Mg–Ca alloy, *J. Mater. Eng. Perform*, 2015, **24**, p 4010–4021
45. S.N. Saud, E. Hamzah, T. Abubakar, H.R. Bakhsheshi-Rad et al., Effects of Mn additions on the structure, mechanical properties, and corrosion behavior of Cu-Al-Ni shape memory alloys, *J. Mater. Eng. Perform*, 2014, **23**, p 3620–3629